Multipath P-Band Interferometry — First Results*

Christoph Hofmann, Marcus Schwäbisch, Susanne Och, Christian Wimmer, João Moreira

Aerosensing Radarsysteme GmbH
c/o DLR, D-82234 Oberpfaffenhofen, Germany
Phone/Fax: +49-8153-281327/-281543
Email: Christoph.Hofmann@dlr.de

Abstract

P-Band interferometric SAR sensors recently have been experienced more attention due to their capability to penetrate vegetation coverage, thus offering the possibility to derive the ground topography of vegetated regions such as forests or agricultural areas. Aerosensing's AeS-1 airborne SAR system operates in its P-Band mode at 415 MHz with a bandwidth of 70 MHz, providing data with a ground resolution of approximately 3 m. Processing of these data needs particular operations in order to face several effects inherent in the airborne repeat-pass characteristic of the sensor. Subject of this paper is the end-to-end interferometric processing chain of AeS-1 data with respect to ground topography estimation. Examples of a flight campaign in Switzerland are given, where elevation measurements have been validated against a high-resolution digital surface model provided by the X-Band subsystem of AeS-1.

1 Introduction

SAR sensors operating in the P-Band range of the microwave spectrum are currently gaining a wider recognition in remote sensing due to their ability to penetrate vegetation coverage. Thus, configuring such a system as a repeat-pass interferometer, the estimation of the pure ground topography becomes feasible as opposed to interferometric systems with higher frequencies which measure the surface elevation or, at best, a mixture of ground and surface elevation. Ground topography together with existing digital surface models furthermore enable the estimation of additional physical parameters like the vegetation canopy height or vegetation biomass, which are currently subject of numerous investigations especially in remote sensing.

Since 1998 Aerosensing Radarsysteme GmbH operates an airborne P-Band SAR with a wavelength of 72 cm and horizontal resolution of about 3 m. Typically, the radar is flown in repeat-pass interferometric mode, yielding as main image products the geocoded digital elevation model and the orthorectified SAR magnitude. This paper gives an overview over the operational data processing chain with respect to ground topography estimation. After a brief description of the radar itself the individual processing steps are illustrated, where special emphasis is put on the P-Band-specific aspects of the procedures. Data from a testsite in Switzerland are presented and finally the results compared to a high resolution digital surface model obtained with the X-Band interferometric subsystem of AeS-1.

2 P-Band Radar System AeS-1

Aerosensing's airborne P-Band SAR is part of the AeS-1 system which additionally includes a X-Band two-antenna interferometric radar [1][2]. It operates at a carrier frequency of 415 MHz and achieves a total range bandwidth of approximately 70 MHz, thus leading to a ground range resolution of about 3 m. Under typical flight conditions, data are gathered at 3 km height, 45° antenna suppression angle, 100 m/s aircraft velocity, and an interferometric baseline of 100 m. The aircraft position is recorded precisely by D-GPS together with an INS and can be estimated to an absolute accuracy of 5...10 cm. The main system parameters are reported in Tab. 1.

*Presented at the Fourth International Airborne Remote Sensing Conference and Exhibition/21st Canadian Symposium on Remote Sensing, Ottawa, Ontario, Canada, 21-24 June 1999.

Table 1: Main system parameters of P-Band AeS-1 SAR

Carrier Frequency	415 MHz
Wavelength	72 cm
Bandwidth	70 MHz
Peak Power	2.5 kW
Polarization	HH
PRF	up to 16 kHz
Incidence Angle (mid range)	45°
Swath Width	1...15 km
Antenna Beamwidth (azimuth)	22°
Horizontal Resolution	3 m × 3 m
Flight Height	500...7000 m
Aircraft Velocity	70...120 m/s

3 Interferometric P-Band SAR Processing

Fig. 1 gives an overview over the entire processing chain from raw data selection up to the generation of georectified image products like the digital elevation model and the radiometrically calibrated SAR magnitude. For processing of extended image strips ($>$ 10 km) the continuous raw data stream is splitted into overlapping parts which are individually fed into the processor and merged just before georectification. Mosaicking of the strips finally leads to entire map sheets. In the following subsections, some of the steps that are especially relevant for P-Band processing are illustrated in more detail.

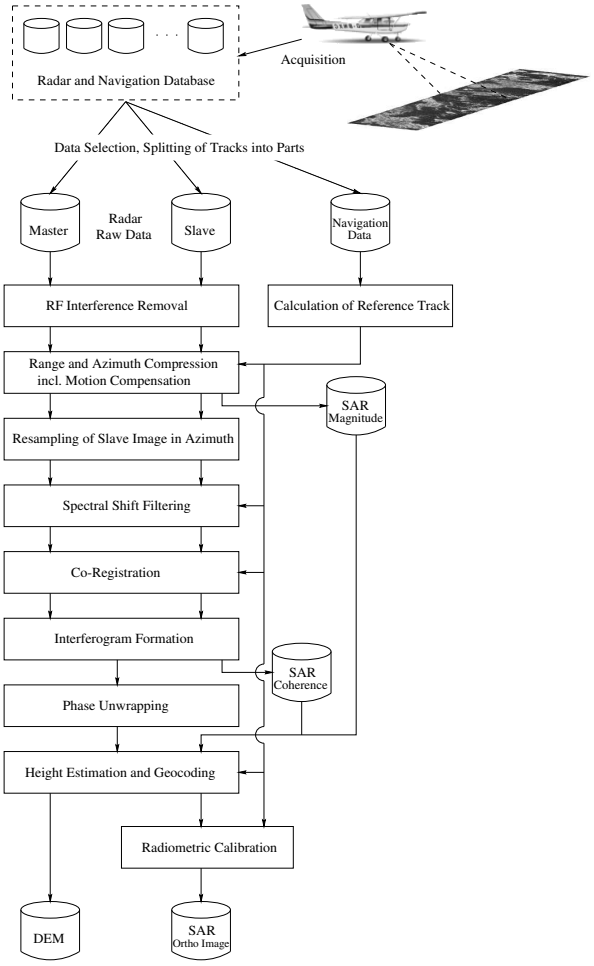

Figure 1: Processing chain for AeS-1 P-Band InSAR data

3.1 RF Interference Removal

RF interference is a common problem in the P-Band frequency range. Due to the high power of AeS-1, distortions are barely visible in the magnitude of the compressed image, but nevertheless are well-pronounced in its phase, a circumstance which complicates the accurate location and hence the removal of the corresponding spectral components in the raw data. Furthermore, in the raw data frequency domain interferences are not present as monochromatic signals of constant amplitude, frequency, and phase in one or more single rangelines as reported by [3].

A Fourier transform of a raw data portion is shown in Fig. 2. Here the interferences are visible as bright spots and as lines in azimuthal direction. Following the work of [4], we split the raw data into overlapping blocks in the spectral domain and average these blocks in azimuthal direction. A typical averaged spectrum is shown in Fig. 4, with the spikes denoting the RF interferences. In order to accurately locate these spikes we first smooth the average with a boxcar (Fig. 5) and then build the difference of both spectra (Fig 6). Now especially small peaks are visible more significantly. Finally, filtering of the rangebins in the spectral domain at the spike locations results in the filtered raw data shown in Fig. 3. As typical block size for averaging we use 2k × 2k samples with an block overlap of 1k.

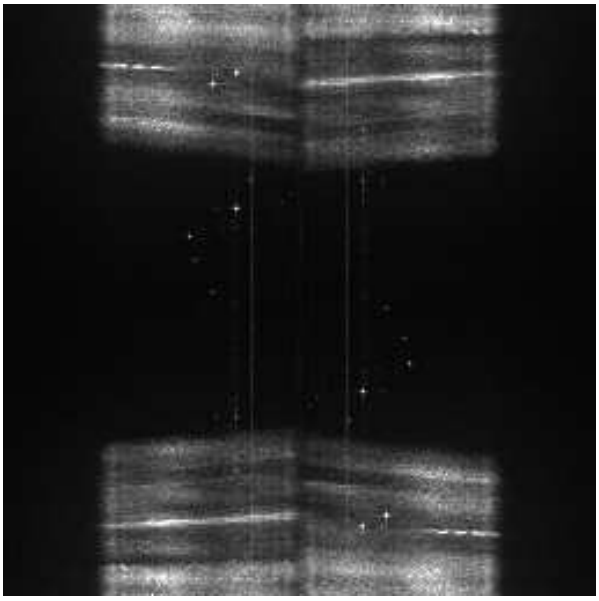

Figure 2: 2k × 2k block of Fourier transformed raw data

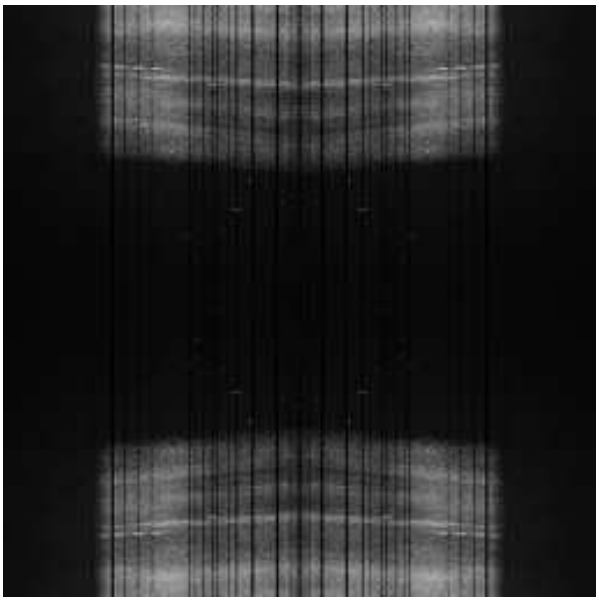

Figure 3: Raw data spectrum after filtering

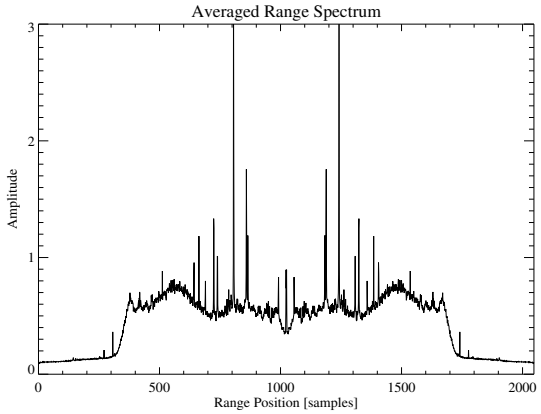

Figure 4: Range spectrum, averaged over 2k range-lines

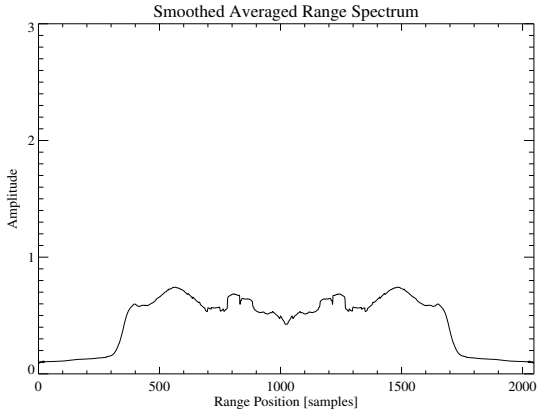

Figure 5: Averaged range spectrum, additionally smoothed

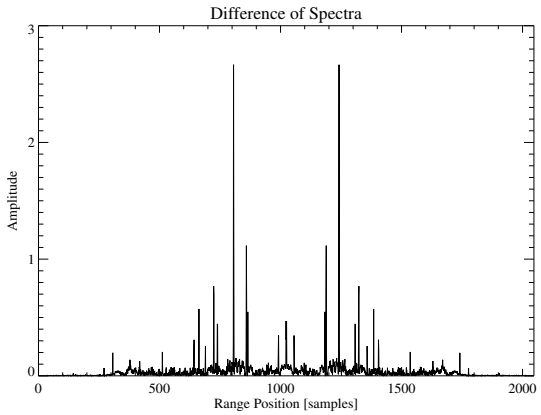

Figure 6: Difference of spectra

3.2 Azimuthal Resampling of Slave Image

Typically, the two data sets used for interferometric processing have been acquired at different aircraft velocities, hence resulting in different azimuth pixel spacings. Before entering the interferometric processor the slave track is resampled onto the spacing of the master track by applying the Shannon interpolation scheme in the frequency domain. Although associated with high computational costs, this operation usually is carried out in order to benefit the image co-registration: correlation results (and hence, registration accuracy) will be much higher if the image samples have the same spatial extension.

3.3 Spectral Shift Filtering

Due to their different observation geometries the interferometric datasets contain different portions of the object's reflectivity spectrum. This spectral shift introduces noise into the interferogram which can be removed by proper bandpass filtering [5]. In the airborne repeat-pass case two aspects are of importance:

- Owing to the large antenna beamwidth in azimuth (Tab. 1) data usually are processed to zero Doppler, disregarding the real antennae squint angles of the two observations without lowering the image quality substantially. Azimuthal filtering consequently becomes superfluous.
- Interferometer geometry in the airborne case results in a highly varying "flat-earth" fringe frequency especially for large baselines (Fig. 7). Additionally, a significant azimuthal component often occurs when flight paths are not parallel. Therefore, filtering should be implemented range- and azimuth-dependent or even slope-adaptive.

3.4 Co-Registration

In contrast to satellite InSAR geometries where the images are shifted (in first order) by a constant value against each other, the airborne case is characterized by a wide dynamical range of shifts from near to far range, dependent mainly on the baseline, wavelength, and image swath width. Fig. 8 gives an example for typical flight conditions of AeS-1 (flight height 3000 m). In order to achieve significant correlation values the image correlation patches have to be kept rather small in range so that the measured shift can be reliably assigned to its center pixel position.

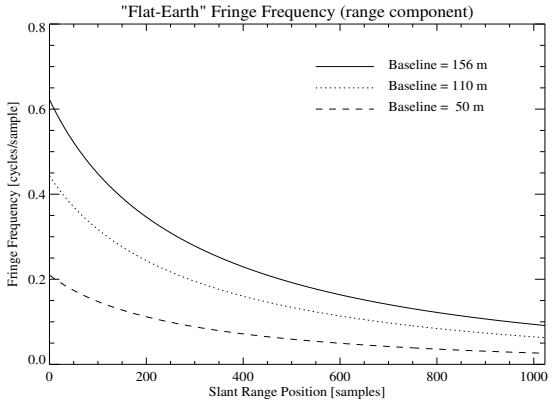

Figure 7: Range component of fringe frequency

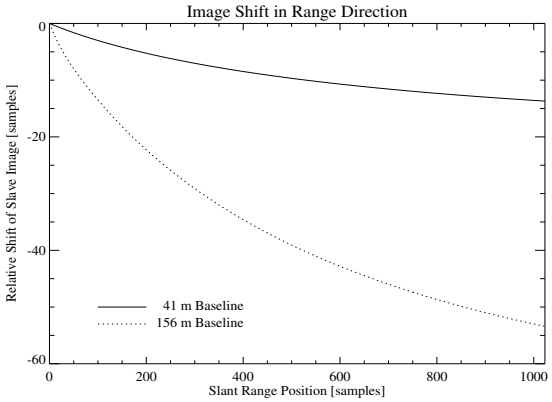

Figure 8: Relative range shift of images as a function of range

4 Results

During an extensive flight campaign in May 1998 in Solothurn/Switzerland, an area of 2 km × 10 km was overflown and imaged 17 times under different viewing angles and from opposite look directions, obtaining baseline combinations in the range of 40...160 m. Fig. 9 gives an example of one image strip, operationally processed to a ground resolution of 2.5 m × 2.5 m.

Figs. 10, 11, and 12 show the coherence, the phase, and the DEM (with amplitude superimposed), resp., of a 2.5 km × 2 km part in the center of the strip, interferometrically generated with 40 m baseline.

Figure 9: 2 km × 10 km strip of SAR magnitude acquired near Solothurn, Switzerland

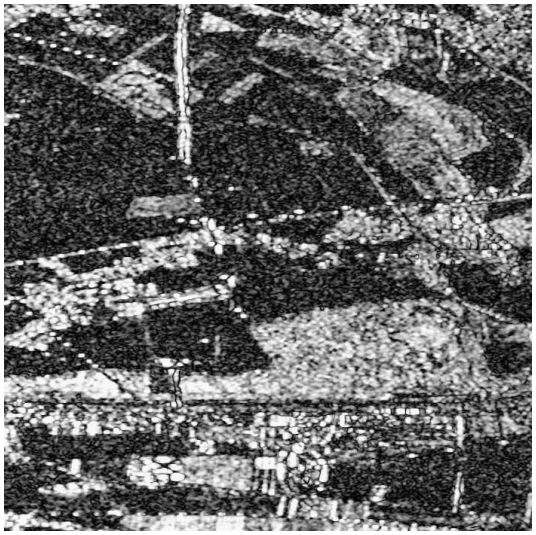

Figure 10: Coherence

Figure 11: Interferometric Phase

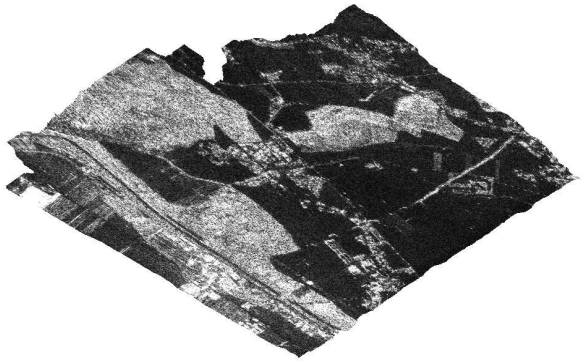

Figure 12: Georectified DEM, with amplitude superimposed

The derived elevation model was compared to a high precision DEM acquired by the X-Band single-pass interferometric subsystem of AeS-1, providing the height of the vegetation surface with an 3σ-accuracy of 1 m [6]. The difference of the two models, shown in Fig. 13, clearly demonstrates the capability of P-Band to penetrate the forest and gather the height information from the ground: the dark areas in Fig. 13, indicating a higher X-Band elevation, exactly correspond to the forested regions of the scene (bright areas in P-Band amplitude of Fig. 9 (central part)). Fig. 14 additionally plots the individual height profiles marked in Fig. 13, depicting three rows of trees with an approximate height of 30 m. The P-Band DEM reaches an overall accuracy of 5 m.

5 Conclusions

As has been shown in the previous sections airborne P-Band SAR interferometry provides a new means for operationally deriving digital models of the pure ground topography with an accuracy in the order of a few meters. Obtainable precision is mainly depending on the configuration of the parameters swath width, baseline, and flight height, which controls the image resolution as well as the power of the received backscatter. Especially smooth surfaces often are characterized by low backscatter and hence poor interferometric phase quality.

Together with the two-antennae single-pass X-Band of AeS-1 the P-Band system now additionally offers the opportunity of deriving vegetation height and biomass, which is currently subject of intensive investigations. Furthermore, research is carried out in the field of radar tomography.

6 References

[1] J. Moreira, "Design of an Airborne Interferometric SAR for High Precision DEM Generation," in *Proceedings of XVIII ISPRS Congress*, vol. XXI, Part B2, Comission II, (Wien), pp. 256–260, 1996.

[2] M. Schwäbisch and J. Moreira, "The High Resolution Airborne Interferometric SAR AeS-1," in *Proceedings of the Fourth International Airborne Remote Sensing Conference*, (Ottawa), 1999.

[3] G. Cazzaniga and A. M. Guarnieri, "Removing RF Interferences from P-Band Airplane SAR Data," in *Proceedings of IGARSS'96*, (Lincoln), pp. 1845–1847, 1996.

[4] S. Buckreuss and R. Horn, "E-SAR P-Band SAR Subsystem Design and RF-Interference Suppression," in *Proceedings of IGARSS'98*, (Seattle), pp. 466–468, 1998.

[5] F. Gatelli, A. M. Guarnieri, F. Parizzi, P. Pasquali, C. Prati, and F. Rocca, "The Wavenumber Shift in SAR Interferometry," *IEEE Trans. on Geoscience and Remote Sensing*, vol. 32, pp. 855–865, July 1994.

[6] E. Meier, "Erfahrungen mit DTMs verschiedener Technologien," in *Fachtagung Digitale Geländemodelle: Technologie und Produkte*, (Zürich), 1999.

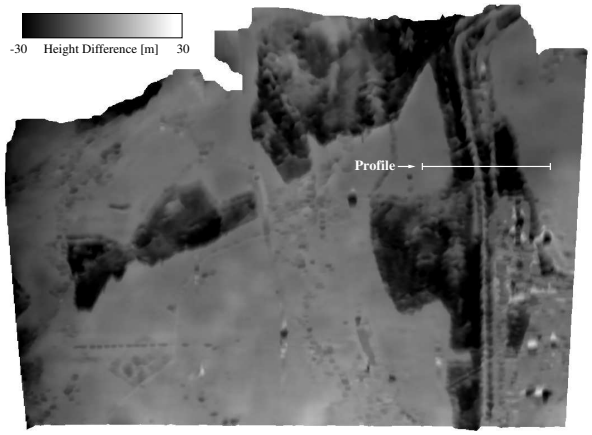

Figure 13: Height difference between P- and X-Band DEM

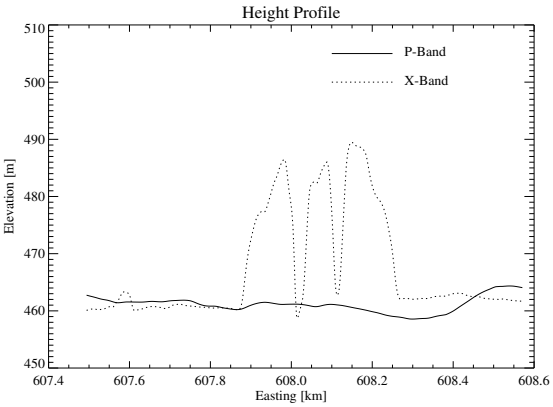

Figure 14: Height profiles corresponding to Fig. 13